Chapter 7

NO_x Storage and Reduction for Diesel Engine Exhaust Aftertreatment

Beñat Pereda-Ayo and Juan R. González-Velasco

Additional information is available at the end of the chapter

http://dx.doi.org/10.5772/55729

1. Introduction

Diesel and lean-burn engines provide better fuel economy and produce lower CO_2 emissions compared to conventional Otto gasoline engines. However, the NO_x gas components in the lean (oxidizing) exhausts from diesel and lean-burn engines cannot be efficiently removed with the classical three-way catalyst (TWC) under operating conditions with excess of oxygen in the exhaust gas. Among the available technologies under research, the NO_x storage-reduction (NSR) catalyst seems to be the most promising method to solve the problem. Basically, NSR catalysts consist of a cordierite monolith washcoated with porous alumina on which an alkali or alkali-earth oxide (e.g. BaO) and a noble metal (Pt) are deposited. These catalysts operate under cyclic conditions. During the lean period, when oxygen is in excess, the platinum oxidizes NO to a mixture of NO and NO_2 (NO_x), which is adsorbed (stored) on Ba as various NO_x species (nitrate, nitrite). During the subsequent short rich period, when some reductant (e.g. H_2) is injected, NO_x ad-species are released and reduced to nitrogen on Pt. Ammonia and N_2O byproduct formation upon NO_x reduction can also be observed over Pt-BaO/Al_2O_3 NSR catalysts.

In this chapter a systematic methodology for preparing Pt-Ba/Al_2O_3 NSR monolith catalysts is presented, the NO_x storage and reduction mechanisms on the catalyst are analysed, and the optimal control of different operational variables to achieve the NSR process with maximum production and selectivity to nitrogen is modeled [1].

2. Historical background

Main pollutants generated in the engine exhaust gases are nitrogen oxides (NO_x), carbon oxides (CO_x), hydrocarbons (HC) and particulate matter (PM). The last term is referred to small particles leaving the engine, mainly constituted by carbonaceous material. These fine

particles can enter into the human lungs, being responsible for some breathing and cardiovascular diseases [2].

The hydrocarbons are organic volatile compounds able to form ozone smog at the ground level when interacting with nitrogen oxides under the sun light. Ozone irritates the eyes, hurts the lungs, causes asthma attack and aggravates other respiratory problems. In addition, ozone is one of the primary components of photochemical smog (or just smog for short). Furthermore, hydrocarbons can also cause cancer [3].

Nitrogen oxides, same as hydrocarbons, are precursors for ozone formation. The NO_2 contributes importantly to the formation of acid rain [4]. The carbon monoxide (CO) reduces the oxygen flow in the blood and results particularly dangerous for people with heart diseases [5]. The carbon dioxide (CO_2) is a greenhouse gas able to make an atmosphere layer trapping the heat and contributing to the global warm of the earth [6].

2.1. Legislation

The negative impacts of those emissions on the human health and the environment and climate have forced legislation to control and limit such emissions. In the U.S.A., NO_x emissions from mobile sources contribute almost 50% of those produced in total, so that more and stricter regulations have been introduced for reducing NO_x emissions from the automobiles [7].

Table 1 shows the most important regulations as introduced by the European Union from the first directive Euro 1 (1992), then Euro 2 (1996), Euro 3 (2000), Euro 4 (2005), Euro 5 (2009), and the most recent Euro 6 (2014) [8]. Emission limits for CO, HC, NO_x, and PM were proposed for petrol and diesel engines. Former regulations limited HC+NO_x jointly, which later were split up into individual HC and NO_x limits.

Step	Date	CO	HC	HC+NO_x	NO_x	PM
			Diesel engines			
Euro 1	07.1992	2.72	—	0.97	—	0.14
Euro 2	01.1996	1.00	—	0.70	—	0.08
Euro 3	01.2000	0.64	—	0.56	0.50	0.05
Euro 4	01.2005	0.50	—	0.30	0.25	0.025
Euro 5	09.2009	0.50	—	0.23	0.18	0.005
Euro 6	09.2014	0.50	—	0.17	0.08	0.005
			Petrol engines			
Euro 1	07.1992	2.72	—	0.97	—	—
Euro 2	01.1996	2.20	—	0.50	—	—
Euro 3	01.2000	2.30	0.20	—	0.15	—
Euro 4	01.2005	1.00	0.10	—	0.08	—
Euro 5	09.2009	1.00	0.10	—	0.06	0.005
Euro 6	09.2014	1.00	0.10	—	0.06	0.005

Table 1. EU emission standards for passenger cars, g km^{-1}.

On the other hand, Euro standards have been completed with stricter regulations for sulphur content in fuels. In fact, the content of S in diesel could not surpass 350 ppm from the year 2000, and only 50 ppm from 2005 (for petrol, 150 ppm in 2000 and 50 ppm in 2005). From 2009, S-free fuels (S ≤ 10 ppm) have been implemented.

In the most recent Euro standards the durability of the catalyst is also specified, e.g. Euro 3 required the emission standards for 80,000 km or 5 years (whatever first occurs). Following regulations required 100,000 km or 5 years. From 2000, with the entrance of Euro 3, vehicles should be equipped with on board diagnostics (OBD), announcing to the driver the system damage or wrong operation, then causing higher emissions which should be avoided.

2.2. Automobile exhaust aftertreatment

More exigent legislation on automobile exhaust emissions has led to the development of aftertreatment systems. Today, three way catalysts (TWC) oxidize CO and HC to CO_2 and H_2O, and simultaneously reduce NO_x to N_2 in a very efficient way for conventional Otto gasoline engines [9-12]. The conventional gasoline engines operate at stoichiometric air/fuel ratio, A/F=14.63 (w/w) [13,14], which produces an exhaust gas with the exact balance of CO, H_2 and HC (reducing species) needed to reduce NO_x and O_2 (oxidizing species). However, diesel engines operate with higher A/F ratios, from 20:1 to 65:1 [15], then producing an exhaust gas with oxygen in excess (Table 2 [16]).

		Conventional gasoline engine	Diesel engine	Lean engine
O_2	%vol.	0.2 – 2	5 – 15	4 – 18
CO_2	%vol.	10 – 13.5	2 – 12	2 – 12
H_2O	%vol.	10 – 12	2 – 10	2 – 12
N_2	%vol.	70 – 75	70 – 75	70 – 75
CO	%vol.	0.1 – 6	0.01 – 0.1	0.04 – 0.08
HC	%vol. C_1	0.5 – 6	0.005 – 0.05	0.002 – 0.015
NO_x	%vol.	0.04 – 0.4	0.003 – 0.06	0.01 – 0.05
SO_x	Related to the content of S in the fuel			

Table 2. Exhaust gas composition, depending on the type of engine.

Fig. 1 shows the conversion curves for each pollutant as a function of the air/fuel ratio, for a TWC. Around the stoichiometric point (A/F=14.63), all the three pollutants (HC, CO and NO) are highly converted (>95%), i.e. they are almost totally removed. However, when the environment is abundant in oxygen as in diesel engines (A/F>20), although this environment enhances the oxidation of HC and CO, the reduction of NO becomes practically inefficient, then this pollutant cannot be appropriately removed with TWC technology [15,17,18].

On the other hand, technical solutions existing for the optimal compromise in removal of NO_x/PM [19], by exhaust gas recirculation (EGR), are not able to achieve the requirements of Euro 6. In fact, in these systems, reduction of PM means eventually an increment of NO_x and

viceversa [20]. Consequently, current technologies combining diesel particulate filters (DPF) and DeNO$_x$ catalysts [21-23] are being reconsidered.

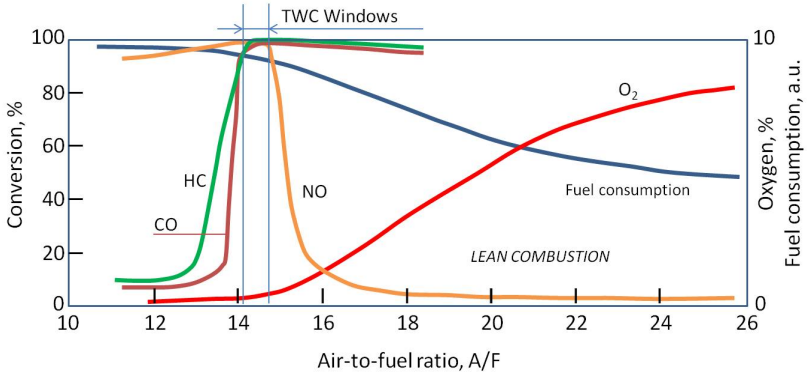

Figure 1. Fuel consumption and TWC behaviour of stoichiometric petrol engines, related to the air-to-fuel ratio.

At present, the removal of NO$_x$ in the diesel engine exhaust gases, mainly in heavy-duty lorries, is controlled by selective catalytic reduction (SCR) with ammonia generated by hydrolysis of urea which must be stored in an on-board container [24,25]. For light vehicles and passenger cars running under lean conditions, the NH$_3$-SCR technology is not appropiate because of the volume of the needed ammonia container. Thus, other technologies are being developped, including the SCR with the presence of reductants in the exhaust, e.g. hydrocarbon [26], and the NO$_x$ storage and reduction (NSR) [27-34], which seems to be the most promising technology and to which is dedicated in this chapter.

2.3. General aspects of the NSR (NO$_x$ Storage and Reduction) catalysis

Up to day, the NSR is considered as the most promising technology for NO$_x$ removal from diesel engine exhaust gases. The corresponding devices are also denominated lean NO$_x$ traps (LNT). Recent excellent revisions can be found in the literature on this technology [34-36]. Following is a brief summary of the chemical principles used in NSR as to facilitate understanding of next sections.

The NSR catalysts run cyclically under lean environment (oxidizing) and rich environment (reducing), being defined by the corresponding A/F ratios. The concept was introduced by Toyota in the middle 90s [27,33]. While running on the road, lean and rich conditions have to be used in an alternative way [37,38]. Under lean conditions, with excess of oxygen (high A/F), NO$_x$ are adsorbed on the catalyst, and then under rich conditions (A/F<14.63) the stored NO$_x$ are released and reduced. Consequently, an NSR catalyst needs sites for NO$_x$ adsorption (alkaline or earth-alkaline compounds) and also sites for NO$_x$ oxidation and/or reduction (noble metals, as in the TWC technology). Most studies in the literature have used storage materials based on Ba. Also other metals such as Na, K, Mg, Sr and Ca have been

used. Thermodynamic and kinetic data demonstrated that basicity of alkaline and earth-alkaline metals is related directly to the NO_x storage capacity, i.e. the storage behavior at 350 °C decreases as follows: K > Ba > Sr ≥ Na > Ca > Li ≥ Mg [34].

The noble metals are normally incorporated with very low percentage, 1-2 wt%. As in the TWC technology, platinum, palladium and rhodium are mostly used [39]. The metal participates into two important steps of the NSR mechanism, the oxidation of NO to NO_2 during the lean period and the reduction of NO_x released during the rich period. In general, it is stablished in the literature that Pt is a good catalyst for NO oxidation, while Rh is more active for NO_x reduction. Obviously, the storage compounds as well as the noble metals should be dispersed on porous materials with high surface area (Al_2O_3, ZrO_2, CeO_2, MgO) washcoated over a monolithic structure, usually cordierite. The most studied formulation in the literature has been Pt-Ba/Al_2O_3, which has also been chosen for this study.

Presently, it is well assumed that the NSR mechanism can be explained by the five following steps, as represented in the upper scheme of Fig. 2 [34,35]:

a. Oxidation of NO to NO_2 (lean conditions, oxidizing environment).
b. Adsorption of NO_x as nitrites or nitrates on the storage sites (lean period, oxidizing environment).
c. Injection and evolution of the used reductant agent (H_2, CO or HC).
d. Release of the stored NO_x from the catalyst surface to the gas stream (rich period, reducing environment).
e. Reduction of NO_x to N_2 (rich period, reducing environment).

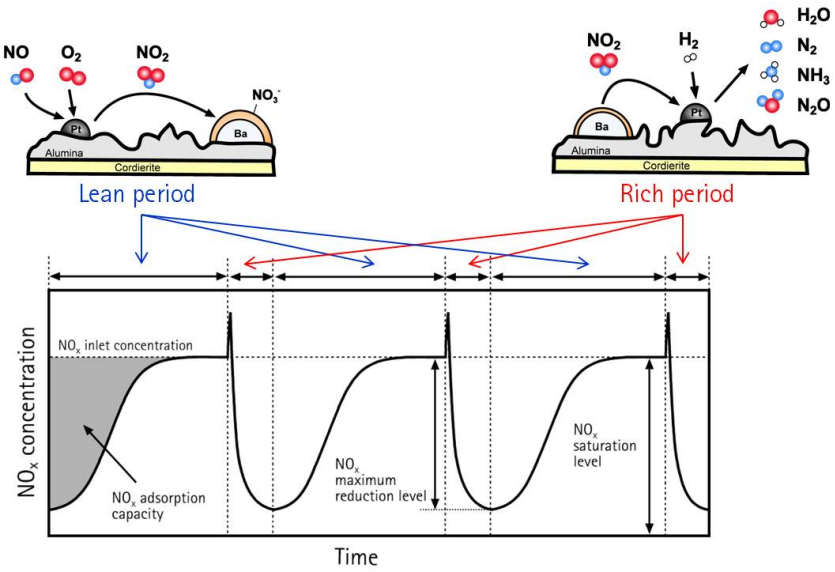

Figure 2. Storage and reduction of NO_x. (a) Schematics of the mechanism; (b) NO_x concentration curves at the exit, during lean and rich periods.

The typical NO_x storage and reduction behaviour can be observed in the bottom graph of Fig. 2. At the beginning of the lean period nearly all the NO_x ($NO+NO_2$) entering the trap is adsorbed, afterwards the NO_x outlet concentration progressively increases due to the successive saturation of the available trapping sites. When saturation is completed, NO_x outlet concentration equals the NO_x inlet concentration. During the subsequent rich period, when H_2 is injected, the adsorbed NO_x species on the catalyst surface react with hydrogen to form N_2O, NH_3 or N_2, resulting in the regeneration of the trap which is again ready for the following lean period.

3. Preparation procedure of monolithic NSR catalysts

Most work dealing with NO_x storage and reduction technology have normally used powder catalyst to carry out different studies. However, for real application, NSR catalysts have to be synthesized in a monolithic structure in order to minimize the pressure drop in the catalytic converter [40-42]. The preparation procedure of powder or monolithic catalysts differs notably. While conventional techniques are used for the incorporation of the active phases in powder catalysts, such as wetness impregnation [43-45], the synthesis of monolithic catalysts requires more sophisticated techniques. This section will be focused on the preparation procedure of monolithic NSR catalysts, paying special attention on their final physico-chemical characteristics (dispersion and distribution of the active phases) and their correlation with the activity for NO_x storage and reduction.

In real application, the mechanical properties of the catalyst are crucial due to the dramatic temperature changes and vibrational strengths that are expected. In this sense, cordierite ($2MgO.2Al_2O_3.5SiO_2$) has been chosen as the base material in automotive application due to its high thermal stability and low expansion coefficient. However, this material exhibits a low surface area which is not suitable for the subsequent incorporation of the active phases. Consequently, the first step of the catalyst preparation consists on the monolithic substrate washcoating with a high surface area oxide, usually alumina.

The most common washcoating procedure is carried out by dipping the monolith into slurry which contains the alumina for washcoating. The monolith is immersed in the slurry for a few seconds and then removed, and the excess of liquid remaining in the channels is blown out with compressed air. This procedure is repeated until the desired Al_2O_3 weight is incorporated as washcoat. It has been previously reported that the characteristics of the final coated monoliths are governed by the properties of the slurry [42], considering as main variables the Al_2O_3 particle size, the Al_2O_3 wt% in the slurry and the pH. Agrafiotis et al. [46] found a threshold value of particle size around 5 μm which is coincident with the size of the cordierite macropores; larger alumina particles do not penetrate into the macropores of the substrate resulting in a poor anchoring of the alumina layer. Therefore, the smaller the particle size in the slurry, the higher the alumina layer anchoring is. In fact, in our previous work [47], the immersion of the monoliths in an alumina slurry with a particle size distribution centered in 1 μm, led to a highly adhered alumina layer, with a weight loss smaller than 0.25% after the washcoated monolith was immersed in ultrasound bath for 15

min. Regarding the Al_2O_3 wt% in the slurry, two contradictory effects are observed. On one hand, as the slurry concentrates in Al_2O_3, few immersions are required to achieve a given amount of washcoated alumina, but on the other hand, the increase in the slurry viscosity resulted in non-homogeneous coating. The influence of the slurry viscosity on the alumina layer homogeneity has been associated with the ease for the suspension excess to be blown out from the monolith channels [48-50]. Another characteristic to be controlled is the stabilization of the alumina slurry so as to avoid the particles from settling down. Nijhuis et al. [41] suggested that addition of some acid to shift pH between 3 and 4 improved the slurry stabilization. Furthermore, the addition of acetic acid up to 2.5 mol l^{-1} (pH=2.6) decreased considerably the viscosity of the slurry, permitting the use of concentrated Al_2O_3 slurries without penalization in the layer homogeneity [47].

Fig. 3 shows the characterization of a washcoated monolith with scanning electron microscopy (SEM). The washcoating procedure was carried out by immersion of the monolith into alumina slurry with the following characteristics: 20 wt% Al_2O_3, mean diameter of 1 μm and 2.5 mol l^{-1} of acetic acid. Eight immersions of the monolith were needed to achieve around 400 mg of Al_2O_3 over the monolithic substrate (D=L=2 cm). Fig. 3a shows a lower magnification image where the intersection of different channels of the monolith can be observed. As it can be clearly noticed, the original structure of the cordierite was completely covered with alumina. The deposition is preferential in the corners of the channels whereas far away from this position, the alumina layer has a constant thickness of 5 μm. Fig. 3b shows a higher magnification image where a crack in the alumina layer is observed. This image also confirms that the alumina layer was composed of particles around 1 μm in size.

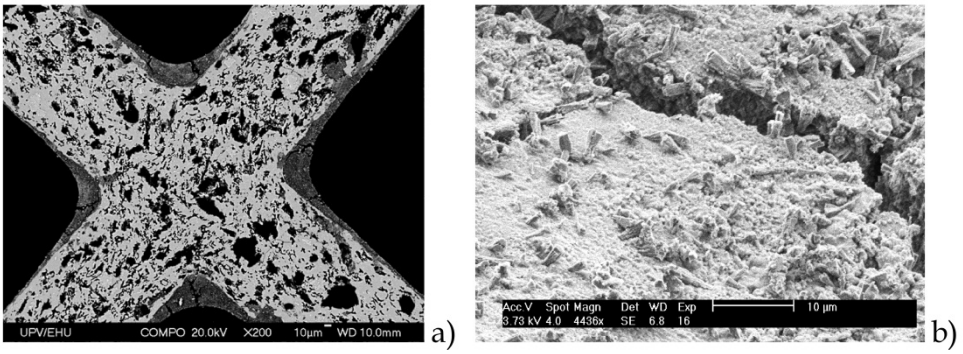

Figure 3. Scanning electron microscoy (SEM) images of the washcoated monolith. (a) Cross section. (b) Higher magnification image of surface in the monolith corner.

The next step in the catalyst preparation is the incorporation of the active phases. As already mentioned, NSR catalysts are usually composed of an alkali or alkali-earth oxide and a noble metal deposited onto the alumina. The most common metal used for NSR catalyst formulation is Pt, whereas BaO is normally used as the storage component [34-36]. The order of the incorporation steps of the active phases Pt and Ba is crucial, especially when

operating at higher temperatures; a higher storage capacity is obtained when impregnating Pt/Al_2O_3 with Ba than when impregnating Ba/Al_2O_3 with Pt, increasing the storage value as much as 54% when adding Ba in the last step [51].

Platinum was incorporated following two different procedures, conventional wetness impregnation (1 monolith) and adsorption from solution (3 monoliths). For the conventional procedure, the channels of the monolith were filled with an aqueous solution containing the desired amount of Pt, using $Pt(NH_3)_4(NO_3)_2$ as a precursor [52]. Then, liquid was evaporated at 80 °C and finally the monolith was calcined at 500 °C for 4 h. On the other hand, in the adsorption from solution procedure, the monoliths were immersed in an aqueous solution with the adequate concentration of Pt. The pH of the solution was turned basic (11.9) in order to generate an electrostatic attraction between the alumina surface, positively charged, and the Pt precursor, negatively charged $Pt(NH_3)_4^{2+}$ [53-55]. The monoliths were maintained immersed in the solution for 24 h so as to reach the adsorption equilibrium. Then, the monoliths were removed from the solution, the excess of liquid blown out and finally the monoliths were calcined at 450, 500 and 550 °C, respectively. The four prepared monolith catalysts were tested for their performance in the NSR process.

Irrespective of the calcination temperature, the monolith prepared by wetness impregnation showed the lowest dispersion of platinum (15%). In the rest of the samples, platinum dispersion decreased as the calcination temperature increased, from 54% at 450 °C to 46% at 500 °C and finally to 19% at 550 °C. Then, 500 °C was chosen as the optimal calcination temperature as a good compromise between platinum dispersion and thermal stabilization of the catalyst. Fig. 4b shows the platinum particle size distribution determined from the transmission electron microscopy image (Fig. 4a) for a Pt/Al_2O_3 sample prepared by adsorption from solution and calcined at 500 °C. As it can be observed, the Pt particles are fairly dispersed over the alumina washcoat with a mean particle size of 1.3 nm.

The last step in the NSR catalyst preparation is the incorporation of the NO_x storage component, i.e. barium. The precursor used was barium acetate [52] and two different procedures were followed: wetness impregnation and incipient wetness impregnation (also known as dry impregnation). For wetness impregnation, the monolith channels were filled with an aqueous solution containing the desired amount of barium. Then, the monolith was dried and calcined. Alternatively, for incipient wetness impregnation, the monolith was immersed in an aqueous solution with an adequate concentration of barium acetate for a few seconds; then, the monolith was removed and the liquid in the channels was blown out with compressed air. Thus only the liquid retained in the pores of the alumina remained in the monolith. In order to determine the distribution of Ba in the catalyst, the monolith was divided into 8 pieces and the content of barium was determined by inductively coupled plasma mass spectrosmetry (ICP-MS). It was found that the distribution of barium resulted in an egg-shell type for wetness impregnation, whereas the incorporation of Ba by incipient wetness impregnation led to more homogenous distribution. Table 3 resumes the preparation procedure, the catalyst physico-chemical characteristics and the NO_x storage achieved with the prepared catalysts (A, B, C and D).

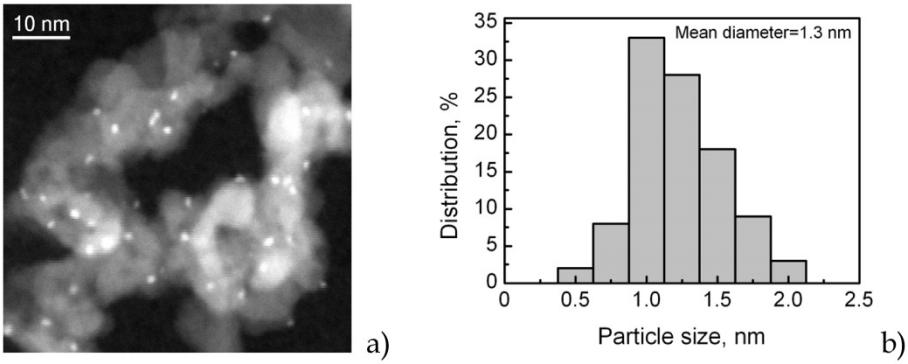

Figure 4. Platinum dispersion measurements. a) Transmision electron microscopy image. b) Platinum particle size distribution.

The activity of the prepared catalysts was tested in a vertical downstream reactor with a feedstream composed of 380 ppm NO and 6% O_2 during the lean period (150 s) and 380 ppm NO and 2.3% H_2 during the rich period (20 s) using nitrogen as the balance gas in both cases. The total flowrate was 3365 ml min^{-1} that corresponds to a gas hourly space velocity (GHSV) of 32,100 h^{-1}. Fig. 5 shows the NO_x concentration profile at the reactor exit for A, B, C and D catalysts. As it can be observed, the NO_x concentration profile is always below the inlet value (380 ppm NO) which evidences the activity of the prepared catalysts for the storage of NO_x. During the storage-reduction cycles, the typical NO_x concentration profile was recorded [56,57]. At the beginning of the lean period practically all the NO_x is stored, and consequently its concentration at the reactor exit is very low. Then, as the lean period time increases, the storage sites become saturated and the NO_x concentration at the reactor exit gradually increases. During the rich period, the NO_x stored are released and reduced with the injected hydrogen, leaving the catalyst surface clean for the subsequent storage period.

	A	B	C	D
Pt incorporation	WI	ADS	ADS	ADS
Calcination T, °C	500	550	500	500
Dispersion,%	15	19	46	46
*Distribution	+	+++	+++	+++
% Pt	0.72	1.43	1.34	1.14
Ba incorporation	WI	WI	WI	DI
*Distribution	+	+	+	++
% BaO	13.1	13.3	16.3	25.2
NO_x storage capacity, %	47.5	55.7	69.6	76.7

Table 3. Preparation procedure, physico-chemical characteristics and NO_x storage capacity for the prepared catalysts A, B, C and D. WI: Wetness impregnation; ADS.: Adsorption from solution; DI: Dry impregnation. The dispersion values are estimated based on powder Pt/Al_2O_3 samples. * Distribution: (+) not good (++) good (+++) very good.

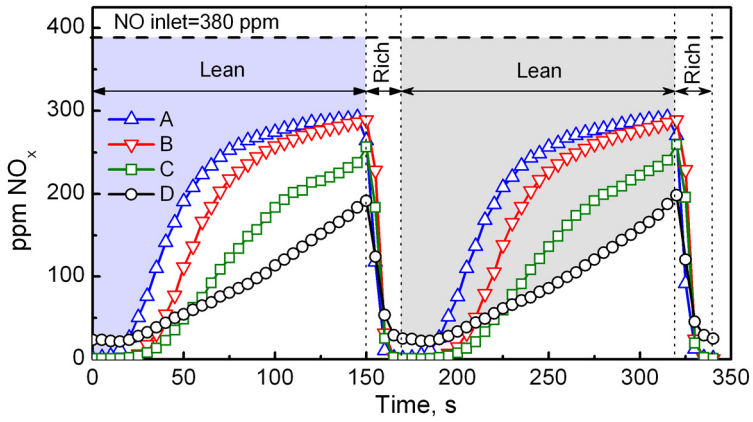

Figure 5. NO_x concentration profile at the reactor exit for two consecutive NO_x storage and reduction cycles for catalysts A, B, C and D.

The NO_x storage capacity is related with the area between the NO inlet level and the NO_x outlet concentration profile; the lower NO_x concentration at the reactor outlet the higher activity of the catalyst for the storage of NO_x. Thus, among the prepared catalysts, catalyst D was found to be the most active (gray area on the rigth graph) and catalyst A (blue area on the left graph). Quantification of the NO_x storage capacity can be found in Table 3 with the following order from the least to the most active: A<B<C<D, according to the physico-chemical characteristics of the samples. It is well known that the Pt-Ba pair is the responsible for the storage of NO_x and that proximity between both metals is beneficial for the process [47,58,59]. Consequently, catalyst A resulted in the less active sample due to the low platinum dispersion and non-homogeneous distribution of both Pt and Ba, as it was prepared by conventional wetness impregnation (WI) of Pt and Ba. For catalyst B, the incorporation of Pt by adsorption from solution (ADS) increased Pt dispersion, but just slightly as the higher calcination temperature (550 °C) also provokes some platinum sintering. Higher Pt loading and dispersion were identified as responsible for better storage capacity, from catalyst A (47.5%) to catalyst B (55.7%). The lower calcination temperature (500 °C) for catalyst C provided much higher dispersion, thus enhancing the NO_x storage capacity up to 69.6%. Furthermore, the incorporation of Ba by dry impregnation (DI) in catalyst D provided a better distribution of barium over the monolith and consequently increased the Pt-Ba proximity resulting in the best storage capacity (76.7%), i.e. 76.7% of NO at the inlet was trapped in the catalyst.

4. The chemistry of NO_x storage and reduction

Many studies are available in the technical literature dealing with the storage step of NSR catalysts. Particularly relevant in this field is research by Forzatti et al. [60-65] and Fridell et al. [66-68]. In situ FTIR spectroscopy has been found to be a very useful tool and several studies have been made on adsorbed NO_x species, though the assignment of peaks is still under debate. Takahashi et al. [27] were pioneers in studying the interaction of NO_x over

NSR catalysts and assigned the 1350 cm^{-1} peak to the nitrate anion. Fig. 6a shows the FTIR spectra of Pt-Ba/Al_2O_3 sample after it was exposed during 20 minutes to a feedstream composed of 440 ppm NO and 7% O_2 using N_2 as the balance gas. As it can be observed, the FTIR spectra changed very significantly with the operating temperature. Bridged nitrites situated at 1220 cm^{-1} [66] were dominant when the adsorption was carried out below 250 °C, whereas the dominant species became ionic nitrates (asymmetric and symmetric modes of monodentate nitrates) located at 1332 and 1414 cm^{-1} [69] for temperatures above 250 °C. This shift in the adsorption mode from nitrites to nitrates with temperature had been already reported in the literature [62,63,66,67,70].

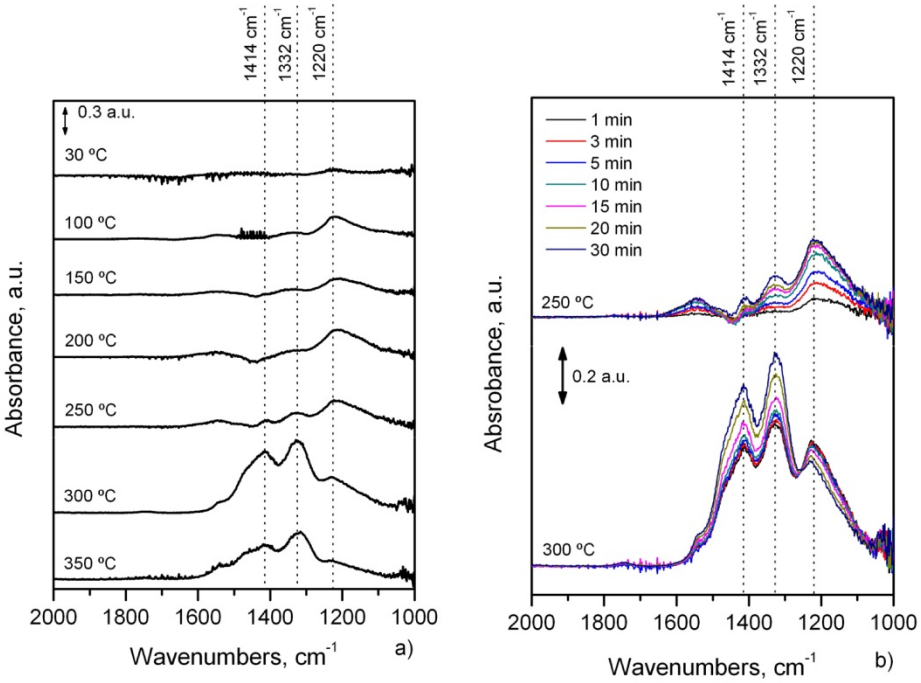

Figure 6. FTIR experiments with powder Pt-BaO/Al_2O_3. (a) Absorbance signals at different temperatures and after 20 min of contact time. (b) Absorbance of the sample at 250 and 300 °C with increasing contact time.

All spectra included in Fig. 6a were recorded after the sample had been exposed to the lean gas mixture for 20 min. However, it can be interesting to examine the evolution of adsorbed species with increasing contact time. Owing to the fact that the adsorption mode of NO_x changed from nitrites at 250 °C to nitrates at 300 °C, several FTIR spectra were recorded at different contact times for those temperatures. The first spectrum was recorded after the sample had been exposed to the lean gas mixture for 1 min while the last one was taken after 30 min. As revealed by Fig. 6b, when the adsorption was carried out at 250 °C nitrite was immediately formed upon admission of NO, whereas nitrate formation was delayed.

Furthermore, the intensity of the peaks corresponding to nitrite (1220 cm^{-1}) and nitrate (1322, 1414 cm^{-1}) increased nearly in the same extent with increasing contact time, which means that there was no conversion from nitrites to nitrates or that conversion from nitrites to nitrates and formation of additional nitrite species occurred simultaneously. In short, below 250 °C nitrite was the dominant adsorption species even at contact times of 30 min, which is much longer than in real operation (1-2 min).

On the other hand, the adsorption pattern resulted completely different at 300 °C (Fig. 6b). From the beginning of the adsorption, the intensity of the bands assigned to ionic nitrates was higher than nitrite. Moreover, it can be noticed that the adsorption peak assigned to nitrites resulted maximum in the first minute of storage and then gradually decreased till minimum after 30 min of contact time. Thus, it can be concluded that there is a shift from nitrite to nitrate when increasing contact time which can be associated with the oxidation of nitrites to nitrates under the lean gas mixture.

In early ages of NSR catalysts, Fridell et al. [66] proposed a three step mechanism in which NO_2 is at first loosely adsorbed on BaO as a BaO-NO_2 species; this species then decomposes to BaO_2 and NO (which is released in the gas phase) and finally barium peroxide reacts with the gas-phase NO_2 to give barium nitrate which can be illustrated as:

$$NO_2 + BaO \rightarrow BaO\text{-}NO_2 \quad (1)$$

$$BaO\text{-}NO_2 \rightarrow BaO_2 + NO \quad (2)$$

$$2NO_2 + BaO_2 \rightarrow Ba(NO_3)_2 \quad (3)$$

The overall stoichiometry of NO_2 adsorption implies the release of one molecule of NO for the consumption of three molecules of NO_2. This reaction is known as the NO_2 disproportionation and has been widely reported for NSR catalysts [62,71-74]:

$$3NO_2 + BaO \rightarrow Ba(NO_3)_2 + NO \quad (4)$$

The formation of nitrate species following the reactions above described, clearly evidences that the oxidation of NO to NO_2 is a preliminar and necessary step for the adsorption of NO. The reaction mechanism used to describe the NO oxidation consists of the following adsorption and desorption steps [75,76]:

$$O_2 + 2Pt \rightarrow 2Pt\text{-}O \quad (5)$$

$$NO + Pt \rightarrow NO\text{-}Pt \quad (6)$$

$$NO + Pt\text{-}O \rightarrow NO_2\text{-}Pt \quad (7)$$

$$NO\text{-}Pt + Pt\text{-}O \rightarrow NO_2\text{-}Pt + Pt \quad (8)$$

$$NO_2\text{-Pt} \rightarrow NO_2\text{+Pt} \tag{9}$$

On the other hand, FTIR experiments showed that apart from nitrates, surface nitrites are also formed during adsorption of NO over the Pt-Ba/Al_2O_3 catalyst. It has been proposed that barium peroxide formed in reaction (2) could also react with NO to form nitrites [62,71,77]:

$$BaO_2\text{+2NO} \rightarrow Ba\left(NO_2\right)_2 \tag{10}$$

BaO_2 can also be formed by an alternative route to reactions (1) and (2), in which NO_2 is not involved, as the following

$$\text{O-Pt+BaO} \rightarrow BaO_2\text{+Pt} \tag{11}$$

The close proximity of BaO to Pt sites promotes spillover of the oxygen adatoms from Pt to BaO. From FTIR spectra shown in Fig. 6a it can be deduced that, at 300 °C, Pt catalyzes the formation of barium nitrate species from nitrite species, which is illustrated as:

$$Ba\left(NO_2\right)_2\text{+2O-Pt} \rightarrow Ba\left(NO_3\right)_2\text{+2Pt} \tag{12}$$

Thus, from the experiments shown in Fig. 6, two parallel routes can be described for the adsorption of NO_x, which are in concordance with the most accepted mechanism by Forzatti et al. [65]. The first route is called "nitrite route" where NO is oxidized at Pt sites and directly stored onto Ba neighbouring sites in the form of nitrite ad-species (reaction 10), which can be progressively transformed into nitrates depending on reaction temperature (reaction 12). The second route is called "nitrate route" which implies the oxidation of NO to NO_2 on Pt sites, followed by NO_2 desproportionation on Ba sites to form nitrates with the giving off NO into the gas phase (reaction 4).

The regeneration step of NSR catalysts is not so well understood as the storage step. Several studies have been published on the chemistry and mechanisms that rule the reduction of NO_x ad-species by H_2. The nitrite and nitrate decomposition can be driven by either the heat generated from the reducing switch [78,79], or the decrease in oxygen concentration that lowers the equilibrium stability of nitrates [34,80]. However, under near isothermal conditions, it has been found that the reduction process is not initiated by the thermal decomposition of the stored nitrates, but rather by a catalytic pathway involving Pt [45]. The reduction of stored nitrates and nitrites leads to the formation of different nitrogen containing species, such as N_2, NH_3 and N_2O along with H_2O. The objective of the NSR operation is to maximize the conversion of NO into N_2, avoiding the formation of NH_3 and N_2O as far as possible. The operational conditions to run efficiently the NSR process are discussed in detail in section 5.

Fig. 7 shows the concentration profiles of NO, NO_2, NH_3, N_2O and H_2O, and the evolution of the MS-signal for N_2, O_2 and H_2 during the regeneration step when the reaction was carried out at 330 °C. The feedstream composition during the lean period was 975 ppm NO, 6% O_2 and Ar to balance, extending the length of this period until complete saturation of the

catalyst was obtained. Afterwards, during the rich period, oxygen was replaced by 0.6% H_2 for 500 s. As can be observed in Fig. 7, before the regeneration period started the sum of NO and NO_2 concentration was close to the inlet value (975 ppm), confirming that the catalyst was saturated. The presence of NO_2 at the reactor exit is due to the oxidation of NO by Pt sites as described in eqns. (5)-(9). When the rich feedstream contacts the catalyst (t=0), the NO and NO_2 concentrations are progressively reduced, eventually reaching 0 ppm. At the very beginning of the rich period a sudden increase in the NO and NO_2 concentrations can be observed due to the release of adsorbed NO_x as a consequence of the decrease in oxygen partial pressure that reduces the stability of the stored nitrates and nitrites. Meanwhile, the incoming H_2 reacts with adsorbed NO_x to form N_2, NH_3 and N_2O. As can be observed in Fig. 7, the formation of N_2 and N_2O is detected immediately after the reduction period started, whereas the detection of H_2O and NH_3 was delayed, the later in a much more extent. On the other hand, the complete consumption of H_2 during the initial period of the regeneration together with the rectangular shape of the H_2O and N_2 formation curve indicates a "plug-flow" type of the regeneration mechanism. As several authors have already reported [45,78,81,82], the hydrogen front travels through the catalyst bed with complete regeneration of the trapping sites as it propagates down the bed with regeneration time. After the required time, complete regeneration of the trap is obtained, i.e. no nitrates or nitrites are present in the catalyst surface, and consequently H_2 is detected at the reactor outlet.

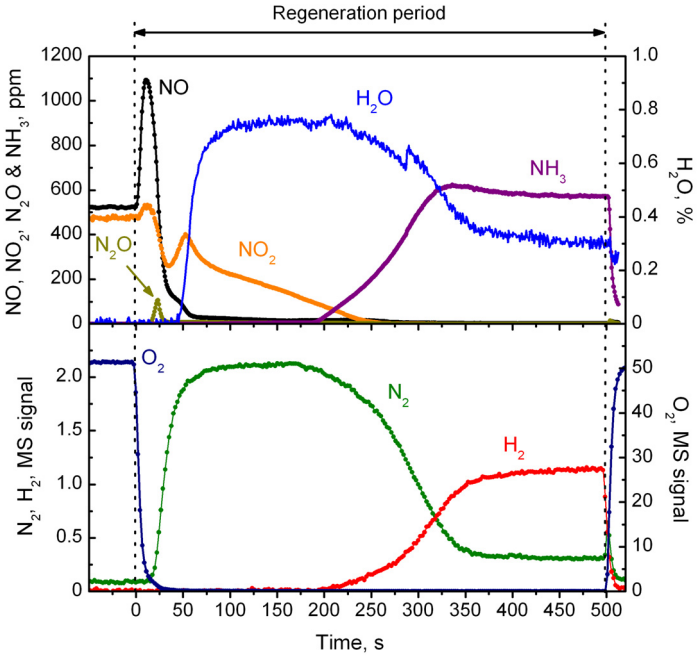

Figure 7. Evolution of NO, NO_2, N_2O, NH_3 and H_2O concentrations by FTIR and MS signals of O_2, N_2 and H_2, during Pt-BaO/Al_2O_3 catalyst regeneration at 330 °C.

The reactants and product profiles shown in Fig. 7 are in agreement with mechanistic aspects of the regeneration already reported [45,81,83,84]. The reduction of stored nitrates with hydrogen has been found to occur by the following reactions:

$$Ba(NO_3)_2 + 8H_2 \rightarrow 2NH_3 + BaO + 5H_2O \quad (13)$$

$$Ba(NO_3)_2 + 5H_2 \rightarrow N_2 + BaO + 5H_2O \quad (14)$$

Lietti et al. [84] reported that during reduction of stored nitrates at 100 °C, reaction (13) accounted for almost all the H_2 consumption, demonstrating that stored nitrates were reduced efficiently and selectively (>90%) to ammonia. On increasing the reduction temperature, nitrogen formation was promoted due to reaction (15) where the formed ammonia continued to react further with stored nitrates to form nitrogen.

$$Ba(NO_3)_2 + 10NH_3 \rightarrow 8N_2 + 3BaO + 15H_2O \quad (15)$$

Thus, nitrogen formation involves a two-step pathway: the fast formation of ammonia by reaction of nitrates with H_2 (reaction 13) and the subsequent conversion of the ammonia formed with stored nitrates leading to the selective formation of N_2 (reaction 15). This overall mechanism for nitrates reduction during LNT regeneration has been confirmed by Pereda-Ayo [85] using isotope labelling techniques and explains the evolution of products at the reactor exit shown in Fig. 7. When the hydrogen front enters the catalyst, the stored NO_x are thought to be converted mainly to ammonia, with total H_2 consumption. Then, the ammonia formed in the regeneration front reacts further with stored nitrates located downstream to give nitrogen. Thus, N_2 is detected as soon as the regeneration period starts, but no ammonia can be detected since it was completely consumed. As the regeneration time increases and the hydrogen front moves forward, the ammonia formed has fewer nitrates to react with, and therefore some NH_3 starts to leave the catalyst unreacted, being detected at the reactor outlet.

5. Analysis of engineering variables of the NSR process

The importance of the catalyst properties, chemical composition, structure, morphology and, in special dispersion and distribution of the metallic phases on its behavior in storing and reducing NO_x has been well reviewed in the work of Roy and Baiker [35]. Generally, research in the scientific open literature has studied independently the two stages, storage and reduction, to advance in the understanding of the mechanisms that happen in each stage. Up to now many papers on the stage of storage have been published [e.g. 60,63,66-68,70,72,87], but notably less on the stage of regeneration (liberation and reduction) [e.g. 39,81,86,88,89]. However, very few studies have considered the whole operation, where the lean and rich periods occur successively as in the real application.

In fact, still scarce relations have been proposed between storage, regeneration and product distribution as determined in laboratory, and the optimization of the conditions in which the

catalytic converter should operate in automobiles. It must be mentioned that engineering parameters, such as gas hourly spatial velocity (GHSV), residence time in the converter, and the lasting time of the periods of storage and regeneration, influence significantly the behavior of lean NO_x traps (LNTs). Kabin et al. [90] studied the storage and reduction of NO_x on model monolithic Pt-BaO/Al_2O_3 catalysts to relate the percentage of the NO_x trapped during storage (trapping efficiency) and the reduced NO_x percentage (average NO_x conversion) with the load of Ba (6-25%) and the GHSV (30,000-120,000 h^{-1}). These authors concluded that the dependence of trapping efficiency on the storage period duration provides a good estimation of the time needed to get a given average conversion during the whole NSR process. More recently, Clayton et al. [91] determined the effects of the catalyst temperature, the composition of the rich stream (NO, H_2, O_2), duration of lean and rich periods and the H_2/NO ratio on the average conversion and product selectivity of a commercial Pt-BaO/Al_2O_3 catalyst. The NO_x average conversion resulted maximum at 300 °C, and also the trapping efficiency resulted maximum at the same temperature. The selectivity to N_2 exhibited a maximum at slightly superior temperature, where the selectivity to NH_3 was minimized.

Thus, to define the optimal operation in the NSR technology, the efficiency of both the storage and reduction steps but also the global NSR efficiency must be studied. This section is devoted to set a definition for the global NSR efficiency of the process, obviously related to the catalyst behavior, the NO_x storage and reduction mechanisms, and the kinetics of the release and reduction of NO_x during the regeneration phase. The defined parameter must account the byproduct formation to maximize the NO_x reduction efficiency towards N_2. The process selectivity depends notably on the lean and rich period duration. For this purpose, experimental runs have been carried out with storage period duration in the order of minutes, followed by rich injection periods during some seconds. The effect of the lean and rich period duration and the reductant concentration should be analyzed, stating as objective functions for optimization the storage capacity in the lean period, the NO_x conversion in the rich period, and the selectivity towards N_2O/NH_3/N_2. Also a bidimensional analysis of operational variables, including temperature and hydrogen concentration, will be made in this section.

The experiments were carried out with a homemade 1.2%Pt-15%BaO/Al_2O_3 monolith catalyst, prepared as explained in section 3 [1,47]. Each time some operational variable was altered, at least ten successive lean-rich cycles were proceeded in order to assure a new stable state of the system, and then the performance was monitored.

5.1. Definition of response parameters

To evaluate the performance of the catalyst during the lean and rich periods the NO_x storage capacity, NO_x conversion and N_2/NH_3 selectivities have been determined from the concentration curves at the reactor exit monitored during the experimental storage-reduction cycles.

The total NO_x stored during the lean period, was calculated as

$$NO_x^{stored}(\mu mol\ NO) = (NO^{in})_L - (NO_x^{out})_L \quad (16)$$

where $(NO^{in})_L$ is the total amount of NO fed during the lean period and $(NO_x^{out})_L$ is the total amount of NO and NO_2 leaving the reactor during the same period. These amounts correspond to the areas graphically represented in Fig. 8, which can be calculated by the corresponding numerical integrations.

When the cumulative NO_x trapped (eqn. 16) is expressed as a percentage of the NO_x fed, then it is referred to as the NO_x storage capacity,

$$\mu_{STO} = \frac{NO_x^{stored}}{(NO^{in})_L} \times 100 \quad (17)$$

The catalyst performance during the rich period was described, on the one hand, by the reduction conversion (X_R) defined as the percentage of NO_x reduced over the total amount of NO_x to be reduced. The latter accounts for the sum of the NO_x stored during the lean period plus the NO continuously fed during the rich period. Then,

$$X_R(\%) = \frac{NO_x^{reduced}}{NO_x^{to\ be\ reduced}} \times 100 = \frac{\left[NO_x^{stored} + (NO^{in})_R\right] - (NO_x^{out})_R}{\left[NO_x^{stored} + (NO^{in})_R\right]} \times 100 \quad (18)$$

On the other hand, the NO_x reduction conversion needs to be complemented with the selectivity to different nitrogen species, including dinitrogen oxide, ammonia and nitrogen. Then, selectivities were defined as

$$S_{NH_3} = \frac{NH_3^{out}}{NH_3^{out} + 2N_2^{out} + 2N_2O^{out}} \times 100 \quad (19)$$

$$S_{N_2O} = \frac{2N_2O^{out}}{NH_3^{out} + 2N_2^{out} + 2N_2O^{out}} \times 100 \quad (20)$$

Fig. 8 shows over a model profile for NO_x and NH_3 molar flows at the exit of the reactor the areas corresponding to the component amounts leaving the reactor during the regeneration period. The N_2O amount leaving the reactor is calculated similarly from the corresponding outlet profile. The FTIR technique is not able to analyze N_2 so that the amount of this component should be calculated from the nitrogen mole balance

$$NO_x^{stored} + (NO^{in})_R = NH_3^{out} + 2N_2^{out} + 2N_2O^{out} + (NO_x^{out})_R \quad (21)$$

i.e. the amount of NO_x stored plus the NO_x amount fed during the lean period equals the NO_x amount leaving the reactor and those amounts converted into NH_3, N_2 and N_2O. Then, the selectivity to N_2 can be expressed as

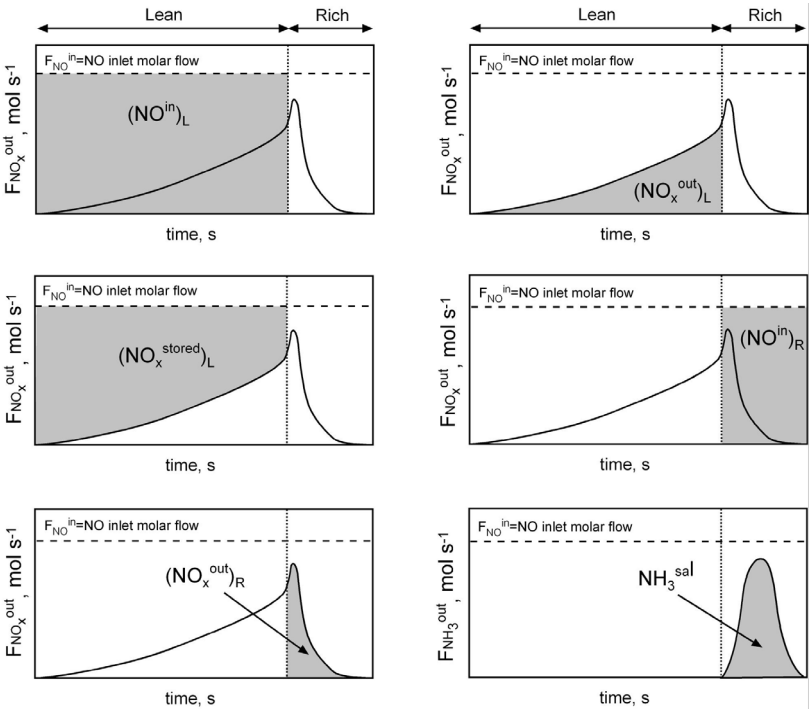

Figure 8. Graphical representation of areas corresponding to magnitudes needed to define parameters for evaluation of the catalyst performance in the NSR process.

$$S_{N_2} = \frac{2N_2}{NH_3^{out} + 2N_2^{out} + 2N_2O^{out}} \times 100 = \frac{\left[NO_x^{stored} + (NO^{in})_R\right] - \left[NH_3^{out} + 2N_2O^{out} + (NO_x^{out})_R\right]}{NH_3^{out} + 2N_2^{out} + 2N_2O^{out}} \times 100 \quad (22)$$

On the other hand, the nitrogen mole balance can be checked if one can determine the amount of N_2 at the reactor exit by the adequate analysis technique, e.g. quantitative mass spectrometry.

The parameters above defined are useful to compare independently the NO_x storage capacity during the lean period and the NO_x reduction conversion during the rich period. The N_2/NH_3 selectivities have been calculated averaged over the whole cycle, as peaks corresponding to those compounds can be seen at the outlet during the rich time but also continuing during the subsequent lean period (see Fig. 9b later). In the case of a conventional Pt–BaO/Al_2O_3 NSR system, the catalyst should operate to exhibit high NO_x storage capacity with also high selectivity to N_2. Thus, definition of a single parameter giving information of the trap performance over the whole storage-reduction cycle would be very convenient to know how efficiently the NSR system is running. This global parameter

should take into account the storage capacity, the reduction conversion and the selectivity of the reaction, giving a general vision of the efficiency of the whole NSR process. Thus, the global NSR efficiency, referred to the N_2 production over the total amount of NO_x fed, can be calculated as

$$\varepsilon_{NSR} = \frac{2N_2^{out}}{(NO^{in})_L + (NO^{in})_R} \times 100 = \frac{2N_2^{out}}{NH_3^{out} + 2N_2^{out} + 2N_2O^{out} + (NO_x^{out})_R} \times 100 \quad (23)$$

5.2. Optimal control of the NSR technology by managing the amount of reductant injected during the regeneration period

NO_x storage-reduction experiments were carried out in a downflow steel reactor. The monolithic catalyst (25 mm in length and diameter, 3.5 g) was placed in the bottom part of the reactor and the set was introduced in a 3-zone oven. The temperature at the entry and exit of the reactor was continuously monitored. The experimental conditions are shown in Table 4. The feedstream during storage was 380 ppm NO/6% O_2/N_2. Gases were fed through mass controllers with a total volumetric flow of 3,365 l min^{-1}, corresponding to a GHSV of 32,000 h^{-1} (STP).

The problem was stated as follows: to find the values of the operational variables, including lasting time of the storage period (lean mixture), lasting time of the regeneration period (rich mixture) and hydrogen concentration injected during the regeneration period, which allow to achieve the maximum NSR efficiency (Eq. 23).

Operational parameters	Values
Temperature, °C	330
Total volumetric flow, l min^{-1} (STP)	3.365
Spatial velocity, GHSV, h^{-1}	32,100
Lean period time duration, s	145, 290, 595
Rich period time duration, s	16 - 47
Lean mixture composition	380 ppm NO, 6% O_2, N_2 to balance
Rich mixture composition	380 ppm NO, 0.41 – 2.36% H_2, N_2 to balance

Table 4. Experimental conditions.

5.2.1. Effect of the H_2 concentration in the regeneration stream on NO_x storage and reduction

Fig. 9 shows the effect of hydrogen concentration in the rich stream on the NO_x and NH_3 concentrations at the exit of the reactor, for experiments carried out at 330 °C. During the lean period the stream composition was 6% O_2 and 380 ppm NO, with N_2 to balance. After 145 s of lean period the oxygen was shifted to hydrogen at different concentrations (0.79, 1.1 and 2.32%), maintaining 380 ppm NO in the feedstream for the regeneration period of 25 s.

The evolution of NO_x concentration at the reactor exit during the storage and regeneration periods is that typical for the NSR process (see Fig. 2), i.e. at the beginning of the lean period all amount of NO_x is stored, and this amount is gradually reduced as the adsorption sites are being saturated, then increasing the NO_x exiting the reactor. It can be seen in Fig. 9a, nevertheless, that the NO_x concentration at the end of the lean period (145 s) did not reach the initial concentration (380 ppm NO), i.e. the catalyst was not completely saturated. The monitored values resulted in 240, 170 and 145 ppm NO_x for runs 1, 2 and 3, respectively.

After 145 s of lean period, the shifting of oxygen by hydrogen to the entry of the reactor provokes the release of the previously stored NO_x which is eventually reduced to N_2O, NH_3 and N_2, according to the mechanisms explained in section 4. The evolution of ammonia concentration at the reactor exit is shown in Fig. 9b. At 330°C, however, N_2O was not practically apreciated at the reactor exit.

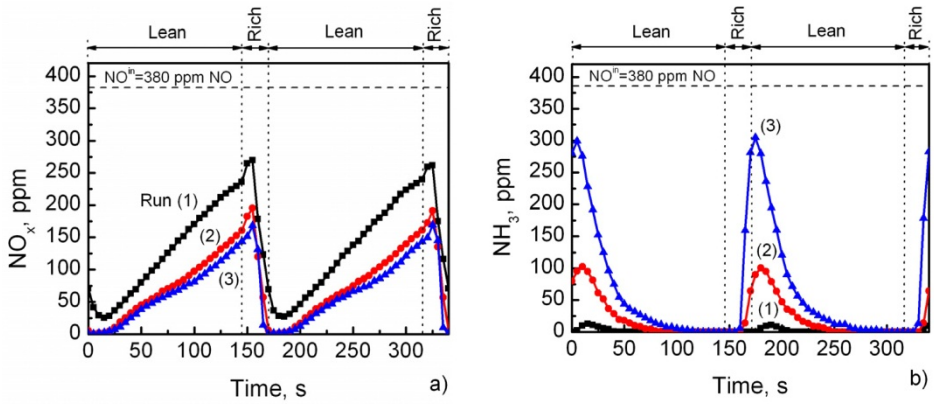

Figure 9. Concentration of (a) NO_x and (b) NH_3 at the reactor exit for two consecutive storage-reduction,for different H_2 concentration during the rich period: (1) 0.79% H_2; (2) 1.1% H_2; (3) 2.32% H_2. t_L=145 s, t_R=25 s.

The hydrogen concentration influences significantly the formation of ammonia at the exit, from 15 ppm NH_3 for 0.79% H_2 to a maximum of 300 ppm NH_3 for 2.32% H_2. In fact, the higher H_2 concentration in the reduction stream the higher NH_3 concentration at the exit, as previously reported [56,78,87-89,91]. These experiments also confirmed the delay in the ammonia detection at the reactor exit related to the beginning of the rich period, as it was observed in the experiments of section 3.

The amount of hydrogen supplied during the rich period also influences the storage capacity and distribution of products. In fact, the storage capacity (μ_{STO}, eqn.17) increased with H_2 concentration, resulting in 40.8, 77.3 y 80.5% for runs 1, 2 and 3, respectively. Similarly, selectivity to NH_3 (S_{NH_3}, eqn. 19) also increased with H_2 concentration, resulting in 2, 10 and 29%, respectively. This influence can be better observed in Fig. 10, where values of the response variables corresponding to additional H_2 concentration experiments have

been included. The response variables calculated have been: storage capacity (μ_{STO}, eqn. 17), NO_x reduction conversion (X_R, eqn. 18), selectivity to N_2 (S_{N_2}, eqn. 22) and NSR efficiency (ε_{NSR}, eqn.23).

Fig. 10a evidences a linear increase of the storage capacity (red line) with H_2 concentration up to 1.1%. Above 1.1% H_2, the storage capacity was maintained almost constant in about 80%. This evolution can be explained from the regeneration mechanism proposed in section 4 [84,85]. During the regeneration step there exits a hydrogen front that travels along the catalyst while regenerating the adsorption sites. If the amount of hydrogen fed is enough, the regeneration front will travel until regeneration of the complete trap. On the contrary, if the reductant is in defect, the regeneration front will not arrive to the final part of the reactor, and the adsorption sites downstream could not be regenerated. This explains that 0.79% H_2 was not able to regenerate the whole catalyst resulting in a limited storage capacity (40.8%). While increasing the H_2 concentration, the regeneration front was able to reach more advanced positions and thus regenerates more adsorption sites, resulting in higher storage capacity during the lean period. Above 1.1% H_2 it is assumed that the regeneration front travels the whole catalyst with total regeneration of the trap. Thus, higher H_2 concentration did not produce significant variations of the storage capacity. Another explanation was supplied by Clayton et al. [86] based on the different storage regions related to the barium phase storage sites based on their proximity to Pt crystallites. They associated the extension of these regions with the platinum dispersion and the reaction temperature.

The reduction conversion (blue line) follows a similar trend to the storage capacity (Fig. 10a). Hydrogen concentration above 1.1% resulted in almost total conversion (97%), whereas lower concentrations resulted also in lower conversion level. In fact, when the supply of H_2 is not enough to allow the hydrogen front achieving the complete regeneration of the trap, e.g. 0.79% H_2, the NO_x reduced/NO_x released ratio is increasing, then decreasing the NO_x reduction conversion to 85%.

Concerning selectivity N_2/NH_3 (remember that N_2O concentration was negligible at 330 °C), Fig. 10a shows that formation of ammonia decreased with lower hydrogen concentration during the rich period, being very low with 0.79% H_2. Thus, when the catalyst regeneration was carried out under low hydrogen concentration (0.79% H_2) the selectivity to N_2 is practically total and only 15 ppm NH_3 were detected. When increasing the H_2 concentration, the selectivity to N_2 decreased progressively in favour of ammonia (Fig. 9b). This agrees with the observation of Clayton et al. [91] that nitrogen selectivity increased with the NO_x/H_2 ratio.

The trends of NO_x storage capacity, NO_x conversion and N_2/NH_3 selectivity above explained, suggest differentiation of two different zones in Fig. 10, limited to each other by 1.1% H_2. In zone A occurs that hydrogen is the reactant that limits the reduction of NO_x, and complete NO_x reduction cannot be achieved (Fig. 8, 0.79% H_2). On the contrary, in zone B the reaction occurs with excess of hydrogen and NO_x are completely reduced. This is also in agreement with the fact that in zone A the NO_x storage capacity is limited as all barium sites cannot be regenerated, whereas in zone B the excess of hydrogen enhances the ammonia formation.

Fig. 10b shows the evaluation of NSR efficiency (ε_{NSR}) with H_2 concentration. As already mentioned, this can be considered as a global parameter that considers the complete storage-reduction cycle as determining the molar amount of nitrogen at the reactor exit over the molar amount of NO at the entry, expressed as percentage. In fact, with some simple mathematical rearrangements of eqns. (17)-(23), the relationship between the NSR efficiency and the previous response variables can be found, which is expressed as:

$$\varepsilon_{NSR} = X_R S_{N_2} (\mu_{STO} \tau_L + \tau_R) \tag{24}$$

where τ_L and τ_R are the dimensionless lean and rich times

$$\tau_L = \frac{t_L}{t_L + t_R} \qquad \tau_R = \frac{t_R}{t_L + t_R} \tag{25}$$

The opposite trend shown by S_{N_2} and μ_{STO} with the amount of hydrogen fed during the rich period (Fig. 10a), makes the NSR efficency to reach a maximum at some intermediate value of %H_2 (eqn. 17), as seen in Fig. 10b. With low %H_2 (zone A) high S_{N_2} is achieved but μ_{STO} is limited, whereas with high %H_2 (zone B) low S_{N_2} (high formation of NH_3) is achieved but μ_{STO} is maintained maximum. Then, the maximum of ε_{NSR} is achieved for 1.1% H_2, just the border between zones A and B, where the amount of hydrogen is that needed to make the complete regeneration of barium sites but not more to avoid formation of ammonia.

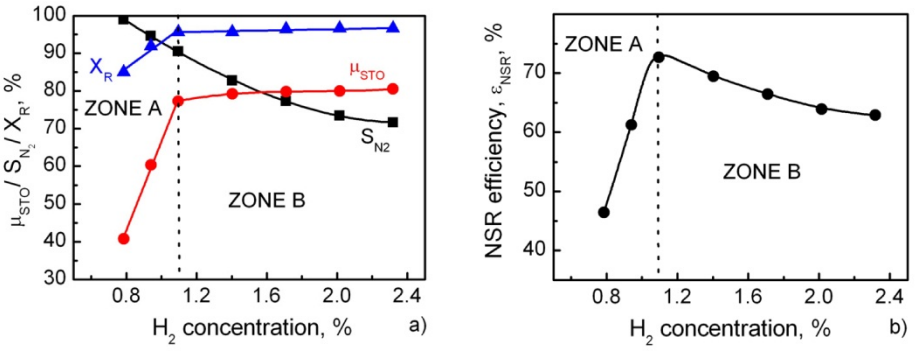

Figure 10. (a) Evolution of the NO_x storage capacity, reduction conversion and selectivity to nitrogen as a function of H_2 concentration during regeneration. (b) NSR efficiency vs. H_2 concentration.

5.2.2. Influence of storage and regeneration period duration on the NO_x storage and reduction

In the previous section all experiments were performed with same duration of the lean and rich periods, i.e. t_L=145 s and t_R=25 s, and varying only the H_2 concentration during the rich period. On the other hand, it can be concluded that the total amount of hydrogen fed during the rich period determines the maximum NSR efficiency. Obviously this amount of

hydrogen can be considered proportional to the product $C_{H_2} \times t_R$, so that it can also be varied by modifying the duration of the rich period. Pereda–Ayo et al. [56] made experiments looking for different combinations of pairs (C_{H_2}, t_R) that achieved maximum NSR efficiency, when the lean period duration was maintained in 145 s. The results of these experiments can be represented as the locus of all these combinations as shown in Fig. 11 (t_L=145 s, red curve) and defines the isocurve of operational conditions to carry out the global NSR process efficiently.

The shape of the isocurve represented in Fig. 11 indicates the inverse relationship between the regeneration time and the reductant concentration to achieve an efficient NSR process, i.e. the shorter reduction time, the higher reductant concentration needed to achieve maximum efficiency. This finding implies again that the supply of the reductant H_2 is controlling the NSR process. This was also observed by Mulla et al. [81] that measured the time required for regenerate the trap catalyst by the width of the N_2 pulse in a mass spectrometer. Analogously, Nova et al. [45] had also noticed that the N_2 production during the regeneration of a Pt–BaO/Al_2O_3 catalyst was limited by the amount of H_2 fed to the reactor.

5.2.3. Extension of the duration of lean period on the NSR performance

To further investigate the optimal conditions to operate the NSR process efficiently, the duration of the storage period was varied, extending the lean period duration from 145 to 290 and 595 s [56]. Again, analogous NO_x storage and reduction experiments were performed with those extended times and the same protocol as before. It has been verified that the same storage capacity was obtained for a given lean period duration, resulting in additional isocurves shown in Fig. 11. As expected, the NO_x storage capacity decreased as the lean period duration increased. When the lean period is longer the catalyst is closer to the saturation level, and consequently the NO_x storage capacity decreases, i.e. 77, 55 and 35% for t_L = 145, 290 and 595 s, respectively. As for selectivity to nitrogen, very similar values were found around 90%, irrespective of the studied variables (C_{H_2}, t_R, t_L), provided that the operation is achieved with maximum efficiency (all points in every isocurve in Fig. 11).

As noted above, the nitrogen production during the regeneration of the catalyst is limited by the amount of hydrogen fed to the reactor. Likewise, increasing the hydrogen supply rate is expected to have a linear effect on the overall rate of NO_x reduction. For our experiments, Fig. 12 shows a linear effect of the hydrogen concentration fed during the rich period on the overall NO_x reduction rate, independent of the duration of the lean period, thus suggesting again that the regeneration step is limited by the amount of hydrogen fed. The linear relationship implies that the time required for complete regeneration should be inversely proportional to the reductant amount of hydrogen fed, as shown in the isocurves of Fig. 11. Mulla et al. [81] also reported the overall rate for NO_x reduction as a linear function of rate of flow of H-atoms in the form of H_2 or NH_3 at 300 °C. Their observations also confirmed that the regeneration process was not mass transfer or kinetically limited, but it was controlled by the supply of the reductant H_2.

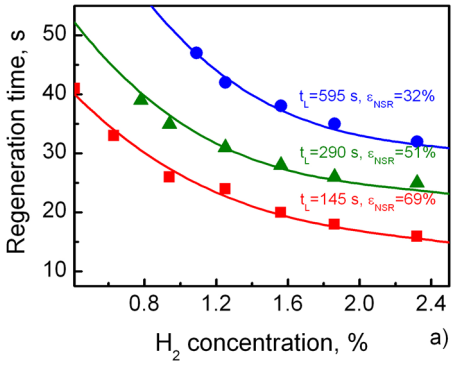

Figure 11. Operation map of the Pt-Ba/Al2O monolithic catalyst. Relationship between operational variables (C_{H_2}, t_P, t_R) for carrying out the NSR process efficiently.

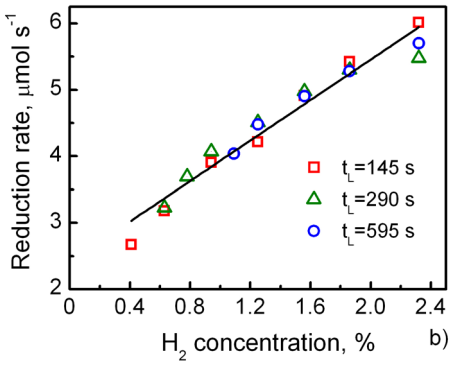

Figure 12. Linear relation between overall NO_x reduction rate *vs.* hydrogen concentraton fed during rich period.

Finally, the term "operation map" is suggested for the set of curves represented in Fig. 11, as a tool for finding any combination of the three studied operational variables: the duration of the lean period, the duration of the rich period and the concentration of the reducing agent: to run the NSR process efficiently. Two ideas may arise from this map. First, every manufactured catalyst can be associated with its own map, so that the comparison of maps will provide information about their relative efficiency when running under the real application. Secondly, one may wonder if any operation point in the map of Fig. 11 is susceptible to be chosen as the best combination (C_{H_2}, t_R, t_L) to run in real application.

5.3. Performance of NO_x storage–reduction catalyst in the temperature–reductant concentration domain by response surface methodology

All previous experiments were carried out at the temperature of 330 °C, at which N_2O at the reactor exit was negligible, thus being selectivity distributed between N_2 and NH_3,

depending on the lean and rich period durations and the hydrogen concentration during the rich period. In this section, the NSR performance trends of the Pt–Ba/Al_2O_3 monolith catalyst will be studied at different temperatures and varying the hydrogen concentration fed during the regeneration period by the response surface methodology (RSM). The NO_x storage and reduction behaviour was tested over 9 levels of temperature: 100, 140, 180, 220, 260, 300, 340, 380 and 420 °C and 9 levels of hydrogen concentration: 0.4, 0.55, 0.7, 0.85, 1, 1.5, 2, 2.5 and 3% [57].

Fig. 13a shows the NO_x storage capacity (μ_{STO}) response surface in the hydrogen concentration and reactor inlet temperature domain. With the aim of finding the optimal region, isocurves corresponding to different levels of μ_{STO} projected to the $T - C_{H_2}$ space are drawn in Fig. 13b. In the region comprised between temperatures of 220 and 260 °C and hydrogen concentrations of 1.75 and 3% a nearly flat surface corresponding to the maximum NO_x storage capacity above 80% is observed (shaded region). These optimal operational conditions correspond to intermediate temperature and excess of hydrogen. At lower temperatures the conversion of NO to NO_2 was not favoured whereas at higher temperatures the stability of the stored nitrates was reduced leading in both cases to a decrease in the NO_x storage capacity [85]. On the other hand, operating with low hydrogen concentration (<1% H_2) resulted also in a sharp decrease in the NO_x storage capacity due to the incomplete regeneration of the catalyst [56].

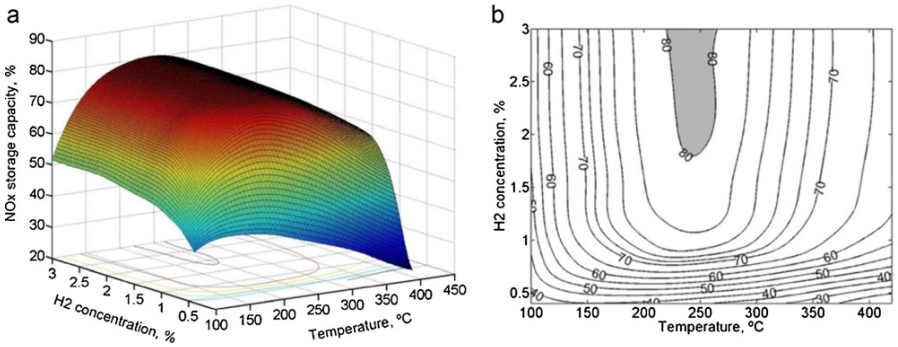

Figure 13. (a) NO_x storage capacity response surface in the temperature and hydrogen dose domain, and (b) isocurves corresponding to different levels of trapping efficiencies projected to the T–C_{H2} space.

Likewise, Fig. 14a shows the selectivity to nitrogen response surface in the hydrogen concentration and temperature domain and Fig. 14b the projected iso-selectivity to nitrogen curves. At low temperature (<150 °C) the selectivity to nitrogen resulted nearly independent of the hydrogen concentration as almost vertical lines can be observed. In this region, the product selectivity changed from N_2O at low H_2 concentrations to NH_3 at higher ones, but remaining practically constant the selectivity to nitrogen. For example, at 100 °C, $N_2O/NH_3/N_2$ = 54.5/5.1/40.4 for 0.4% H_2; $N_2O/NH_3/N_2$ = 34.7/33.1/33.2 for 1% H_2; $N_2O/NH_3/N_2$ = 19.5/48.8/31.7 for 3% H_2. For higher temperatures (>180 °C), where the formation of N_2O was negligible, the influence of hydrogen concentration on the selectivity

to nitrogen became markedly significant. In this region, the higher hydrogen concentration the lower nitrogen selectivity, and therefore the higher ammonia, was obtained. For example, at 340 °C, $N_2O/NH_3/N_2$ = 3.4/2.2/94.5 for 0.4% H_2; $N_2O/NH_3/N_2$ = 0.8/9.4/89.9 for 1% H_2; $N_2O/NH_3/N_2$ = 0.6/25.0/74.4 for 3% H_2.

The optimal operational window which resulted in a selectivity to nitrogen higher than 90% was situated at intermediate-high temperatures (T >250 °C) and low hydrogen concentrations (C_{H_2} < 1%) as it can be seen in Fig. 14b (shaded region).

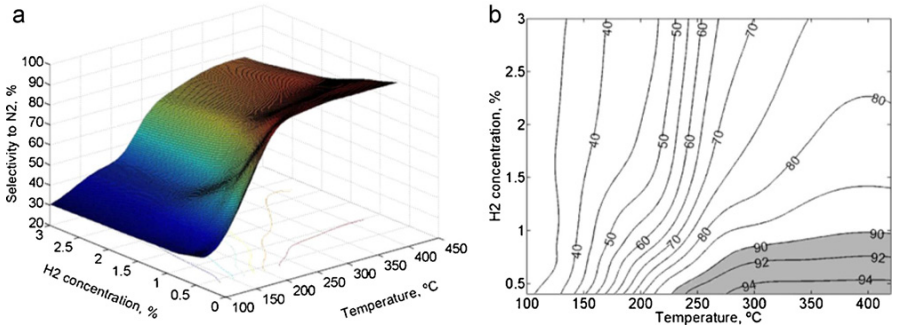

Figure 14. (a) Selectivity to N_2 response surface in the temperature and hydrogen dose domain, and (b) isocurves corresponding to different levels of nitrogen selectivity projected to the T–C_{H2} space.

The optimal operating region for maximizing NO_x trapping efficiency and nitrogen selectivity, Fig. 13b and 14b, respectively, did not intercept to each other. The first was maximum at intermediate temperatures and high H_2 concentrations, T = 220–260 °C and C_{H2} = 1.75–3% H_2; whereas the selectivity to nitrogen was favoured by high temperatures and low H_2 concentrations, T > 250 °C and C_{H_2} < 1%.

In conventional NSR systems NO_x conversion towards N_2 should be maximized while NH_3 formation should be avoided. The percentage of NO_x converted into nitrogen relative to the total amount of NO entering the trap has been defined as global NSR efficiency (ε_{NSR}, eqn. 23), which allows one to look for the optimal combination of reactor inlet temperature and hydrogen concentration during rich period to obtain the most efficient NSR operation. Fig. 15a shows the ε_{NSR} surface response in the hydrogen concentration and temperature domain and Fig. 15b the projected iso-efficiency curves. As it could be expected, an optimal interval of temperature and hydrogen concentration situated between the optimal operational conditions to obtain maximum storage and maximum selectivity was found. The NSR efficiency resulted higher than 60%, that is, more than 60% of NO entering the trap was converted into nitrogen, in the following operating window: T = 250–350 °C and C_{H_2} = 0.8–1.5. This region provides the best compromise between NO_x storage capacity and selectivity to N_2 to maximize the nitrogen production at the reactor exit related to the total amount of NO at the reactor inlet. The most efficient operation corresponds to 0.9% H_2 and 280 °C reaching 65% of global NSR efficiency (Fig. 15b).

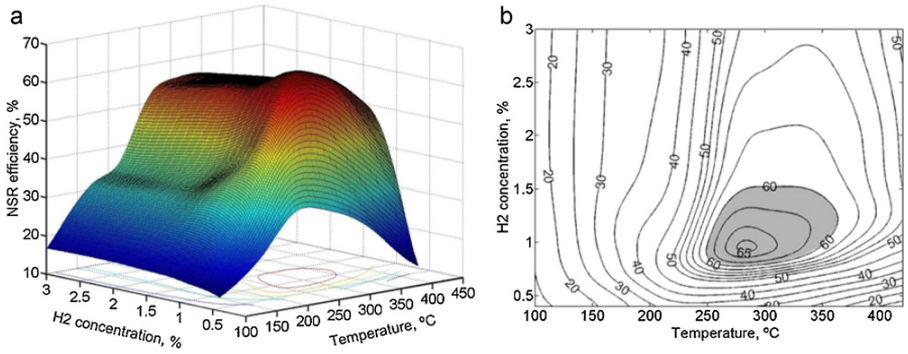

Figure 15. (a) Global NSR efficiency response surface in the temperature and hydrogen dose domain, and (b) isocurves corresponding to different levels of NSR efficiencies projected to the T–C_{H2} space.

6. Conclusions

The NO_x storage and reduction technology for diesel eshaust aftertreatment has been studied in the present chapter, including the synthesis of Pt-BaO/Al_2O_3 monolith catalyst, the involved reaction mechanisms or chemistry of the process, and the control of engineering parameters, of importance in the real application in automobiles, to remove nitrogen oxides most efficiently by conversion to nitrogen.

The preparation methodology for Pt-BaO/Al_2O_3 monolith catalyst has been described. The monolith is primarily washcoated with a thin film of porous alumina. Then platinum is incorporated by adsorption (ion exchange) from a $Pt(NH_3)_4(NO_3)_2$ aqueous solution. Finally, the barium as NO_x storage component is incorporated by dry impregnation from a $Ba(CH_3COO)_2$ aqueous solution. This procedure achieves homogeneous distribution as well as high dispersion of platinum and barium on the catalyst surface, then providing the adequate Pt-Ba proximity which enhances the interaction needed for Pt to promote both the initial NO oxidation and the reduction of N_xO_y adspecies on the Ba sites.

The chemistry of NO_x regeneration and reduction mechanisms has been reviewed. Operando FTIR experiments of NO_x adsorption on powder Pt-Ba/Al_2O_3 samples has shown that below 250 °C nitrite species are predominant whereas above 250 °C nitrate species are predominant. Thus, two parallel routes have been verified. The "nitrite route" where NO is oxidized on Pt sites and stored onto Ba neighbouring sites in the form of nitrite ad-species which can progressively transform into nitrates depending on the reaction temperature. The second route, called "nitrate route" implies the oxidation of NO to NO_2 on Pt, then NO_2 desproportionation on Ba to form nitrates NO evolved into the gas phase.

During the regeneration period, when oxygen is shifted by hydrogen, the reduction of stored nitrites and nitrates leads to the formation of different nitrogen containing species, namely N_2, N_2O and NH_3 along with water. Nitrogen formation involves first the fast formation of ammonia by reaction of nitrates with H_2 and then the subsequent conversion of

the ammonia formed with stored nitrates leading to the selective formation of N_2. At temperature above 330 °C, N_2O was almost negligible.

In the automobile practice, the operational conditions at which the process is conducted affect significantly the NSR behaviour of a Pt-BaO/Al_2O_3 monolith catalyst, such as the duration of lean and rich periods and the concentration of reductant fed during the regeneration period. There exists a given amount of hydrogen which is needed to achieve the complete reduction of NO_x (stored during the lean period and fed during the rich period). Below that minimum, as regeneration is not complete the reduction conversion is lower and consequently the storage capacity in the subsequent lean period is also reduced. However, with hydrogen in defect very high selectivity towards N_2 is achieved. On the other hand, with hydrogen in excess the formation of ammonia increases notably, although NO_x storage capacity is practically maintained at maximum and almost total reduction conversion is achieved. The maximum global NSR efficiency (percentage of N_2 at the exit related to NO at the entry) is achieved just at the stoichiometric point, when the amount of H_2 is neither in defect nor in excess. The amount of hydrogen fed during the rich period is proportional to the product $C_{H_2} \times t_R$ so that this amount can be controlled by managing either H_2 concentration or duration of the regeneration period. In fact, there exist different combinations (C_{H_2}, t_R) which achieve similar NSR efficiency. The locus of these combinations conforms the isoeffiency curve map with NSR efficiency as the response parameter.

The combined analysis of temperature (100-420 °C) and H_2 concentration (0.4-3%), maintaining lean and rich period times in 145 and 25 s respectively, has allowed to find the maximum storage capacity at intermediate temperature (~240 °C) and high reductant concentration (>2% H_2). Maximum selectivity to N_2 has been obtained operating at high temperature (>300 °C) and hydrogen in defect (<1% H_2). The optimal control is performed at intermediate position, i.e. 270 °C and 1% H_2, at which the maximum global NSR efficieny is achieved.

Nomenclature

Abreviations

ADS	Adsorption from solution, catalyst preparation procedure.
DI	Dry impregnation
FTIR	Fourier Transform Infrared spectroscopy.
ICP-MS	Inductively Coupled Plasma Mass Spectroscopy.
LNT	Lean NO_x Trap.
MS	Mass Spectroscopy.
NSR	NO_x Storage and Reduction.
PM	Particulate matter.
RSM	Response Surface Methodology.
SEM-EDX	Scanning Electronic Microscopy-Energy Dispersed X-Ray Spectroscopy.
SCR	Selective Catalytic Reduction.

STP	Standard temperature and pressure
TEM	Transmission Electronic Microscopy.
TWC	Three way catalyst.
WI	Wet impregnation, catalyst preparation procedure.

Variables

A/F	Air-to-fuel ratio.
C_{H_2}	Concentration of the reductant agent (hydrogen) in the regeneration feedstream, %.
NO_x	Nitrogen oxides (NO+NO_2).
NO_x^{stored}	Amount of NO_x stored, mol s^{-1}.
$(NO^{in})_L$	Total amount of NO fed to the system during the duration of lean period (storage), mol.
$(NO_x^{out})_L$	Total amount of NO_x at the exit of reactor during the duration of lean period (storage), mol.
$(NO^{in})_R$	Total amount of NO fed to the system during the duration of rich period (regeneration), mol.
$(NO_x^{out})_R$	Total amount of NO_x at the exit of reactor during the duration of rich period (regeneration), mol.
S_{N_2}	Selectivity towards nitrogen, eqn. (22), %.
S_{N_2O}	Selectivity towards N_2O, eqn. (20), %.
S_{NH_3}	Selectividad towards ammonia, eqn. (19), %.
T	Temperature, °C.
t_L	Lasting time of lean period (storage), s.
t_R	Lasting time of rich period (regeneration), s.
X_R	NO_x conversion during the regeneration period, eqn. (18), %.

Greek symbols

ε_{NSR}	Global NSR efficiency, eqn. (23) , %.
μ_{STO}	NO_x storage capacity, eqn. (17), %.
τ_L	dimensionless lean period time
τ_R	dimensionless rich period time

Author details

Beñat Pereda-Ayo and Juan R. González-Velasco*
Department of Chemical Engineering, Faculty of Science and Technology, University of the Basque Country UPV/EHU, Bilbao, Spain

* Corresponding Author

Acknowledgement

The authors wish to acknowledge the financial support provided by the Spanish Science and Innovation Ministry (CTQ2009-125117) and the Basque Government (Consolidated Research Group, GIC 07/67-JT-450-07).

7. References

[1] Pereda-Ayo B. NO_x storage and reduction (NSR) for diesel engines: synthesis of Pt-Ba/Al_2O_3 monolith catalyst, reaction mechanisms and optimal control of the process. PhD Thesis, University of the Basque Country, Bilbao, Spain; 2012.

[2] Mazzarella G, Ferraraccio F, Prati MV, Annunziata S, Bianco A, Mezzogiorno A, Liguori G, Angelillo IF, Cazzola M. Effects of diesel exhaust particles on human lung epithelial cells: An in vitro study. Respiratory Medicine 2007;101 1155-1162.

[3] Derwent RG. The long-range transport of ozone within Europe and its control. Environmental Pollution 1990; 299-318.

[4] Parvulescu VI, Grange P, Delmon B. Catalytic removal of NO. Catalysis Today 1998;46 233-316.

[5] Folinsbee LJ. Human health-effects of air-pollution. Environmental Health Perspectives 1993;100 45-56.

[6] Krupa SV, Kickert RN. The greenhouse effect - impacts of ultraviolet-B (Uv-B) radiation, carbon-dioxide (CO_2), and ozone (O_3) on vegetation. Environmental Pollution 1989;61 263-393.

[7] Klingstedt F, Arve K, Eranen K, Murzin DY. Toward improved catalytic low-temperature NO_x removal in diesel-powered vehicles. Accounts of Chemical Research 2006;39 273-282.

[8] Dieselnet. Emission standards. European Union. Cars and light trucks. http://www.dieselnet.com/standards/eu/ld.php (accessed 1 May 2012).

[9] Taylor KC. Nitric-oxide catalysis in automotive exhaust systems. Catalysis Reviews Science Eng. 1993;35 457-481.

[10] Tamaru K, Mills GA. Catalysts for control of exhaust emissions. Catalysis Today 1994;22 349-360.

[11] Heck RM, Farrauto, RJ. Automobile exhaust catalysts. Applied Catalysis A: General 2001;221 443-457.

[12] González-Velasco JR, Entrena J, González-Marcos JA, Gutiérrez-Ortiz JI, Gutiérrez-Ortiz MA. Preparation, activity and durability of promoted platinum catalysts for automotive exhaust control. Applied Catalysis B: Environmental 1994;3 191-204.

[13] Numan JG, Robota HJ, Cohn MJ, Bradley SA. Physicochemical properties of Ce-containing three-way catalysts and the effect of Ce on catalyst activity. Journal of Catalysis 1992;133 309-324.

[14] Engler BH, Lindner D, Lox ES, Schäfer-Sindlinger, Ostgathe K. Development of improved Pd-only and Pd/Rh three-way catalysts. Studies in Surface Science and Catalysis 1995;96 441-460.

[15] Heck RM, Farrauto RJ, Gulati S. Catalytic Air Pollution Control: Commercial Technology. New Yersey: John Wiley & Sons; 2009.

[16] Seijger GBF. Cerium-ferrierite catalyst systems for reduction of NO_x in lean burn engine exhaust gas. PhD Thesis, Technical University Delft, Delft, Netherlands; 2002.

[17] González-Velasco JR, González-Marcos MP, Gutiérrez-Ortiz MA, Botas-Echevarría JA. Catálisis, automóvil y medio ambiente. Anales de Química 2002;4 24-35.

[18] Basile F, Fomasari G, Grimandi A, Livi M, Vaccari A. Effect of Mg, Ca and Ba on the Pt-catalyst for NOx storage reduction. Applied Catalysis B: Environmental 2006;69 58-64.

[19] Trichard JM. Current tasks and challenges for exhaust after-treatment research: An industrial viewpoint. Studies in Surface Science and Catalysis 2007;171 211-233.

[20] Centi G, Perathoner S. Introduction: State of the art in the development of catalytic processes for the selective catalytic reduction of NO_x into N_2. Studies in Surface Science and Catalysis 2007;171 1-23.

[21] Johnson TV. Review of diesel emissions and control. International Journal of Engine Research 2009;10 275-285.

[22] Maricq MM. Chemical characterization of particulate emissions from diesel engines: A review. Journal of Aerosol Science 2007;38 1079-1118.

[23] Fino D. Diesel emission control: Catalytic filters for particulate removal. Science and Technology of Advanced Materials 2007;8 93-100.

[24] Biswas S, Verma V, Schauer JJ, Sioutas C. Chemical speciation of PM emissions from heavy-duty diesel vehicles equipped with diesel particulate filter (DPF) and selective catalytic reduction (SCR) retrofits. Atmospheric Environment 2009;43 1917-1925.

[25] Brandenberger S, Krocher O, Tissler A, Althoff R. The state of the art in selective catalytic reduction of NO_x by ammonia using metal-exchanged zeolite catalysts. Catalysis Reviews, Science and Engineering 2008;50 492-531.

[26] Amiridis MD, Zhang TJ, Farrauto RJ. Selective catalytic reduction of nitric oxide by hydrocarbons. Applied Catalysis B: Environmental 1996;10 203-227.

[27] Takahashi N, Shinjoh H, Iijima T, Suzuki T, Yamazaki K, Yokota K, Suzuki H, Miyoshi N, Matsumoto S, Tanizawa T, Tanaka T, Tateishi S, Kasahara K. The new concept 3-way catalyst for automotive lean-burn engine: NO_x storage and reduction catalyst. Catalysis Today 1996;27 63-69.

[28] Matsumoto SI. Recent advances in automobile exhaust catalysts. Catalysis Today 2004;90 183-190.

[29] Belton DN, Taylor KC. Automobile exhaust emission control by catalysts. Current Opinion in Solid State & Materials Science 1999;4 97-102.

[30] Alkemade UG, Schumann B. Engines and exhaust after treatment systems for future automotive applications. Solid State Ionics 2006;177 2291-2296.

[31] Twigg MV. Progress and future challenges in controlling automotive exhaust gas emissions. Applied Catalysis B: Environmental 2007;70 2-15.

[32] Fridell E., Skoglundh M., Johansson S., Westerberg BR, Törncrona A, Smedler G. Investigations of NO_x storage catalysts. Studies in Surface Science and Catalysis 1998;116 537-547.

[33] Miyoshi N, Matsumoto S, Katoh T, Tanaka T, Harada J, Takahashi N, Yokota K, Sugiara M, Kasahara K. Development of new concept three-way catalyst for automotive lean-burn engines. SAE Technical Paper Series 950809; 1995.

[34] Epling WS, Campbell LE, Yezerets A, Currier NW, Parks JE. Overview of the fundamental reactions and degradation mechanisms of NO_x storage/reduction catalysts. Catalysis Reviews, Science and Engineering 2004;46 163-245.

[35] Roy S, Baiker A. NO_x Storage-reduction catalysis: from mechanism and materials properties to storage-reduction performance. Chemical Reviews 2009;109 4054-4091.

[36] Liu G, Gao PX. A review on NO_x storage/reduction catalysts: mechanism, materials and degradation studies. Catalysis Science & Technology 2011;1 552-568.

[37] Li YJ, Roth S, Dettling J, Beutel T. Effects of lean/rich timing and nature of reductant on the performance of a NO_x trap catalyst. Topics in Catalysis 2001;16 139-144.

[38] Epling WS, Yezerets A, Currier NW. The effect of exothermic reactions during regeneration on the NO_x trapping efficiency of a NO_x storage/reduction catalyst. Catalysis Letters 2006;110 143-148.

[39] Abdulhamid H, Fridell E, Skoglundh M. The reduction phase in NO_x storage catalysis: Effect of type of precious metal and reducing agent. Applied Catalysis B: Environmental 2006;62 319-328.

[40] Meille V. Review on methods to deposit catalysts on structured surfaces. Applied Catalysis A: General 2006;315 1-17.

[41] Nijhuis TA, Beers AEW, Vergunst T, Hoek I, Kapteijn F, Moulijn JA. Preparation of monolithic catalysts. Catalysis Reviews, Science and Engineering 2001;43 345-380.

[42] Avila P, Montes M, Miro E. Monolithic reactors for environmental applications - A review on preparation technologies. Chemical Engineering Journal 2005;109 11-36.

[43] Piacentini M, Maciejewski M, Baiker A. NO_x storage-reduction behavior of Pt-Ba/MO_2 (MO_2 = SiO_2, CeO_2, ZrO_2) catalysts. Applied Catalysis B: Environmental 2007;72 105-117.

[44] Malpartida I, Vargas MAL, Alemany LJ, Finocchio E, Busca G. Pt-Ba-Al_2O_3 for NO_x storage and reduction: Characterization of the dispersed species. Applied Catalysis B: Environmental 2008;80 214-225.

[45] Nova I, Lietti L, Forzatti P. Mechanistic aspects of the reduction of stored NO_x over Pt-Ba/Al_2O_3 lean NO_x trap systems. Catalysis Today 2008;136 128-135.

[46] Agrafiotis C, Tsetsekou A. The effect of powder characteristics on washcoat duality. Part I: Alumina washcoats. Journal of the European Ceramic Society 2000;20 815-824.

[47] Pereda-Ayo B, López-Fonseca R, González-Velasco JR. Influence of the preparation procedure of NSR monolithic catalysts on the Pt-Ba dispersion and distribution. Applied Catalysis A: General 2009;363 73-80.

[48] Tsetsekou A, Agrafiotis C, Milias A. Optimization of the rheological properties of alumina slurries for ceramic processing applications - Part I: Slip-casting. Journal of the European Ceramic Society 2001;21 363-373.

[49] Valentini M, Groppi G, Cristiani C, Levi M, Tronconi E, Forzatti P. The deposition of gamma-Al_2O_3 layers on ceramic and metallic supports for the preparation of structured catalysts. Catalysis Today 2001;69 307-314.

[50] Agrafiotis C, Tsetsekou A. Deposition of meso-porous gamma-alumina coatings on ceramic honeycombs by sol-gel methods. Journal of the European Ceramic Society 2002;22 423-434.

[51] Lindholm A, Currier NW, Dawody J, Hidayat A, Li J, Yezerets A, Olsson L. The influence of the preparation procedure on the storage and regeneration behavior of Pt and Ba based NO_x storage and reduction catalysts. Applied Catalysis B: Environmental 2009;88 240-248.

[52] Pereda-Ayo B, Duraiswami D, López-Fonseca R, González-Velasco JR. Influence of platinum and barium precursors on the NSR behavior of Pt-Ba/Al_2O_3 monoliths for lean-burn engines. Catalysis Today 2009;147 244-249.

[53] Regalbuto JR, Agashe K, Navada A, Bricker ML, Chen Q. A scientific description of Pt adsorption onto alumina. Studies in Surface Science and Catalysis 1998;118 147-156.

[54] Spieker WA, Regalbuto JR. A fundamental model of platinum impregnation onto alumina. Chemical Engineering Science 2001;56 3491-3504.

[55] Regalbuto JR, Navada A, Shadid S, Bricker ML, Chen Q. An experimental verification of the physical nature of Pt adsorption onto alumina. Journal of Catalysis 1999;184 335-348.

[56] Pereda-Ayo B, Duraiswami D, Delgado JJ, López-Fonseca R, Calvino JJ, Bernal S, González-Velasco JR. Tuning operational conditions for efficient NO_x storage and reduction over a Pt-Ba/Al_2O_3 monolith catalyst. Applied Catalysis B: Environmental 2010;96 329-337.

[57] Pereda-Ayo B, Duraiswami D, González-Marcos JA, González-Velasco JR. Performance of NO_x storage-reduction catalyst in the temperature-reductant concentration domain by response surface methodology. Chemical Engineering Journal 2011;169 58-67.

[58] Cant NW, Liu IOY, Patterson MJ. The effect of proximity between Pt and BaO on uptake, release, and reduction of NO_x on storage catalysts. Journal of Catalysis 2006;243 309-317.

[59] Clayton RD, Harold MP, Balakotaiah V, Wan CZ. Pt dispersion effects during NO_x storage and reduction on Pt/BaO/Al_2O_3 catalysts. Applied Catalysis B: Environmental 2009;90 662-676.

[60] Nova I, Castoldi L, Lietti L, Tronconi E, Forzatti P, Prinetto F, Ghiotti G. NO_x adsorption study over Pt-Ba/alumina catalysts: FT-IR and pulse experiments. Journal of Catalysis 2004;222 377-388.

[61] Nova I, Castoldi L, Lietti L, Tronconi E, Forzatti P. On the dynamic behavior of "NO_x-storage/reduction" Pt-Ba/Al_2O_3 catalyst. Catalysis Today 2002;75 431-437.

[62] Lietti L, Forzatti P, Nova I, Tronconi E. NO_x Storage Reduction over Pt---Ba/[gamma]-Al_2O_3 Catalyst. Journal of Catalysis 2001;204 175-191.

[63] Prinetto F, Ghiotti G, Nova I, Lietti L, Tronconi E, Forzatti P. FT-IR and TPD investigation of the NO_x storage properties of BaO/Al_2O_3 and Pt-BaO/Al_2O_3 catalysts. Journal of Physical Chemistry B 2001;105 12732-12745.

[64] Nova I, Castoldi L, Prinetto F, Dal Santo V, Lietti L, Tronconi E, Forzatti P, Ghiotti G, Psaro R, Recchia S. NO_x adsorption study over Pt-Ba/alumina catalysts: FT-IR and reactivity study. Topics in Catalysis 2004;30-1 181-186.

[65] Forzatti P, Castoldi L, Nova I, Lietti L, Tronconi E. NO_x removal catalysis under lean conditions. Catalysis Today 2006;117 316-320.

[66] Fridell E, Skoglundh M, Westerberg B, Johansson S, Smedler G. NO_x storage in barium-containing catalysts. Journal of Catalysis 1999;183 196-209.

[67] Broqvist P, Gronbeck H, Fridell E, Panas I. NO_x storage on BaO: theory and experiment. Catalysis Today 2004;96 71-78.

[68] Westerberg BR, Fridell E. A transient FTIR study of species formed during NO_x storage in the Pt/BaO/Al_2O_3 system. Journal of Molecular Catalysis A: Chemical 2001;165 249-263.

[69] Szanyi J, Kwak JH, Hanson J, Wang CM, Szailer T, Peden CHF. Changing morphology of BaO/Al_2O_3 during NO_2 uptake and release. Journal of Physical Chemistry B 2005;109 7339-7344.

[70] Elizundia U, Lopez-Fonseca R, Landa I, Gutierrez-Ortiz MA, Gonzalez-Velasco JR. FT-IR study of NO_x storage mechanism over Pt/BaO/Al_2O_3 catalysts. Effect of the Pt-BaO interaction. Topics in Catalysis 2007;42-43 37-41.

[71] Mahzoul H, Brilhac JF, Gilot P. Experimental and mechanistic study of NO_x adsorption over NO_x trap catalysts. Applied Catalysis B: Environmental 1999;20 47-55.

[72] Cant NW, Patterson MJ. The storage of nitrogen oxides on alumina-supported barium oxide. Catalysis Today 2002;73 271-278.

[73] Kikuyama S, Matsukuma I, Kikuchi R, Sasaki K, Eguchi K. A role of components in Pt-ZrO_2/Al_2O_3 as a sorbent for removal of NO and NO_2. Applied Catalysis A: General 2002;226 23-30.

[74] Rodrigues F, Juste L, Potvin C, Tempere JF, Blanchard G, Djega-Mariadassou G. NO_x storage on barium-containing three-way catalyst in the presence of CO_2. Catalysis Letters 2001;72 59-64.

[75] Olsson L, Persson H, Fridell E, Skoglundh M, Andersson B. Kinetic study of NO oxidation and NO_x storage on Pt/Al_2O_3 and Pt/BaO/Al_2O_3. Journal of Physical Chemistry B 2001;105 6895-6906.

[76] Olsson L, Westerberg B, Persson H, Fridell E, Skoglundh M, Andersson B. A kinetic study of oxygen adsorption/desorption and NO oxidation over Pt/Al_2O_3 catalysts. Journal of Physical Chemistry B 1999;103 10433-10439.

[77] Li XG, Meng M, Lin PY, Fu YL, Hu TD, Xie YN, Zhang J. Study on the properties and mechanisms for NO_x storage over Pt/$BaAl_2O_4$-Al_2O_3 catalyst. Topics in Catalysis 2003;22 111-115.

[78] Cumaranatunge L, Mulla SS, Yezerets A, Currier NW, Delgass WN, Ribeiro FH. Ammonia is a hydrogen carrier in the regeneration of Pt/BaO/Al_2O_3 NO_x traps with H_2. Journal of Catalysis 2007;246 29-34.

[79] Medhekar V, Balakotaiah V, Harold MP. TAP study of NO_x storage and reduction on Pt/Al_2O_3 and Pt/Ba/Al_2O_3. Catalysis Today 2007;121 226-236.

[80] Liu ZQ, Anderson JA. Influence of reductant on the thermal stability of stored NO_x in Pt/Ba/Al_2O_3 NO_x storage and reduction traps. Journal of Catalysis 2004;224 18-27.

[81] Mulla SS, Chaugule SS, Yezerets A, Currier NW, Delgass WN, Ribeiro FH. Regeneration mechanism of Pt/BaO/Al_2O_3 lean NO_x trap catalyst with H_2", Catalysis Today 2008;136 136-145.

[82] Partridge WP, Choi JS. NH_3 formation and utilization in regeneration of Pt/Ba/Al_2O_3 NO_x storage-reduction catalyst with H_2. Applied Catalysis B: Environmental 2009;91 144-151.

[83] Nova I, Lietti L, Castoldi L, Tronconi E, Forzatti P. New insights in the NO_x reduction mechanism with H_2 over Pt-Ba/gamma-Al_2O_3 lean NO_x trap catalysts under near-isothermal conditions. Journal of Catalysis 2006;239 244-254.

[84] Pereda-Ayo B, González-Velasco JR, Burch R, Hardacre C, Chansai S. Regeneration mechanism of a Lean NO_x Trap (LNT) catalyst in the presence of NO investigated using isotope labelling techniques. Journal of Catalysis 2012;285 177-186.

[85] Lietti L, Nova I, Forzatti P. Role of ammonia in the reduction by hydrogen of NO_x stored over Pt-Ba/Al_2O_3 lean NO_x trap catalysts. Journal of Catalysis 2008;257 270-282.

[86] Clayton RD, Harold MP, Balakotaiah V. NO_x storage and reduction with H_2 on Pt/BaO/Al_2O_3 monolith: Spatio-temporal resolution of product distribution. Applied Catalysis B: Environmental 2008;84 616-630.

[87] Lindholm A, Currier NW, Fridell E, Yezerets A, Olsson L. NO_x storage and reduction over Pt based catalysts with hydrogen as the reducing agent. Influence of H_2O and CO_2. Applied Catalysis B: Environmental 2007;75 78-87.

[88] Epling WS, Yezerets A, Currier NW. The effects of regeneration conditions on NO_x and NH_3 release from NO_x storage/reduction catalysts. Applied Catalysis B: Environmental 2007;74 117-129.

[89] Nova I, Castoldi L, Lietti L, Tronconi E, Forzatti P. How to control the selectivity in the reduction of NO_x with H_2 over Pt-Ba/Al_2O_3 Lean NO_x Trap catalysts. Topics in Catalysis 2007;42-43 21-25.

[90] Kabin KS, Muncrief RL, Harold MP,Li YJ. Dynamics of storage and reaction in a monolith reactor: lean NO_x reduction. Chemical Engineering Science 2004;59 5319-5327.

[91] Clayton RD, Harold MP, Balakotaiah V. Performance Features of Pt/BaO Lean NO_x Trap with Hydrogen as Reductant. Aiche Journal 2009;55 687-700.